Title

Evaluating Electrically-Heated Versus Conventionally-Heated Steam Methane Reforming

Author

Chheda, Parth Jagdish

Publication Date

2024

Peer reviewed|Thesis/dissertation

UNIVERSITY OF CALIFORNIA

Los Angeles

Evaluating Electrically-Heated Versus Conventionally-Heated Steam Methane Reforming

A thesis submitted in partial satisfaction of the
requirements for the degree Master of Science
in Chemical Engineering

by

Parth Jagdish Chheda

2024

ABSTRACT OF THE THESIS

Evaluating Electrically-Heated Versus Conventionally-Heated Steam Methane Reforming

by

Parth Jagdish Chheda
Master of Science in Chemical Engineering
University of California, Los Angeles, 2024
Professor Panagiotis D. Christofides, Chair

Steam methane reforming (SMR) is the most widely used hydrogen (H_2) production method, converting natural gas and steam into H_2 and carbon dioxide (CO_2). SMR is a mature industrial technology that burns fossil fuels to provide heat to the endothermic reforming reactions and to generate steam, which contributes to the production of greenhouse gas emissions. In order to reduce heating-based emissions, an electrically-heated steam methane reforming process has been proposed. Conventional SMR uses a packed bed catalyst and receives heat through radiation from hot flames in the surrounding furnace; on the other hand, an electrified SMR employs a washcoated catalyst, and is resistively-heated through the wall of the reactor coil. To gain further insight into the scalability of hydrogen production processes using electrically-heated reformers, this thesis takes experimental data from an electrified reformer built at UCLA, extracts kinetic parameters, and uses these parameters to model a hydrogen production plant with a hydrogen production capacity of 253 $\mathrm{kg/h}$ (2623 $\mathrm{Nm^3/h}$). The simulated plant includes a reformer, two shift reactors, pressure swing adsorption (PSA) for separation, and a heat exchange network to make steam for

the reformer. A sensitivity analysis is conducted for the most energy-efficient H_2 production conditions (e.g., operating pressure, heat flux), and CO_2 production amounts are compared to a conventional SMR process, demonstrating that electrified SMR can potentially be a significantly cleaner alternative.

The thesis of Parth Jagdish Chheda is approved.

Dante A. Simonetti

Carlos Gilberto Morales Guio

Panagiotis D. Christofides, Committee Chair

University of California, Los Angeles

2024

Contents

List of Figures

List of Tables

ACKNOWLEDGMENTS

I would like to thank my advisor Professor Panagiotis D. Christofides for his guidance and support during the course of my research.

I would like to thank Professors Carlos Gilberto Morales Guio and Dante A. Simonetti for reviewing my thesis and contributing to my Master's thesis committee.

Finally, I would like to thank my parents and my partner for helping me through this journey without whom this would not have been possible.

This work was submitted under the title "Modeling and Design of a Combined Electrified Steam Methane Reforming-Pressure Swing Adsorption Process" for publication in Chemical Engineering Research and Design, and is co-authored by Esther Hsu, Dominic Peters, Berkay Çıtmacı, Xiaodong Cui, Yifei Wang, Professor Carlos G. Morales-Guio and Professor Panagiotis D. Christofides. I would like to acknowledge their contributions to my thesis and extend my profound gratitude for their support and help.

Chapter 1

Introduction

Hydrogen (H_2) has been widely recognized as an ideal energy carrier [1] that only generates water as exhaust upon combustion or oxidation in a fuel cell. Over 95% of H_2 is currently produced through conventional steam methane reforming (SMR) or coal gasification processes [2]. Depending on the carbon dioxide (CO_2) emissions associated with each H_2 manufacturing process, H_2 is given different color labels. H_2 generated via reforming of natural gas and coal is referred to as grey and brown hydrogen, respectively, to highlight the environmental drawbacks of these production methods. If the accompanying CO_2 is captured and sequestered, then it is labeled as blue H_2. In contrast, green hydrogen, produced from renewable electricity using clean technologies such as water electrolysis, offers a sustainable alternative to the production of carbon-free hydrogen. However, the scale of green hydrogen production remains limited due to challenges with the scale-up of electrolyzer-based manufacturing plants. Therefore, alternative approaches to reduce the emission of CO_2 associated with the production of H_2 are required. One available strategy is to improve conventional hydrogen production methods through the electrification of the steam methane reforming step.

Steam methane reforming, the most common process for industrial-scale H_2 production, is a net endothermic chemical process that generates H_2 from methane (CH_4) and steam at high

temperatures [3]. The byproducts, carbon monoxide (CO) and CO_2, must then be separated in an H_2 purification unit. Consequently, a typical SMR-based industrial H_2 production plant comprises of: the reforming reactor, the water-gas shift reactor, a network of heat exchangers for the cooling of the raw gas and the production of steam, and a gas purification unit (e.g., [4]).

For the reforming process, conventional SMR plants typically employ multiple reactor coils packed with a nickel-based catalyst, which are heated by a furnace fueled by the combustion of a portion of the feed (typically natural gas), and the burning of off-gas fuels. The combustion of at least 0.11 kg of methane is required to provide the energy to process 1 kg of methane feed in the reformer when using a steam-to-carbon ratio (S/C) of 3 [5]. As a result, fossil fuel-based heating of the reformer is unsustainable as it leads to significant CO_2 emissions from hydrocarbon combustion. Moreover, heat transfer via radiation from burner flames in the furnace creates non-uniform heat gradients, leading to lower energy utilization, decreased process yields, and lower methane conversion [6]. To address these issues, traditional heating can be replaced with electrical resistive heating, also known as Joule-heating, since the heating efficiency for resistively-heated reformers nears 100% [7]. At UCLA, an electrically-heated experimental SMR setup was constructed to aid in the development of modeling and control strategies [8, 9, 10] that may be integral to the scale-up of this novel reforming method. However, the reformer is just one of the units of the SMR plant. The convective section in a conventional reformer generates the much-needed steam to power compression work in the rest of the plant, and also is used to burn and recover energy from the off-gas of the separation unit. Electrification of the radiant section of the reformer requires a new approach to energy integration for the plant and the treatment of off-gases, different from that of conventional hydrogen plants. The design and simulation of H_2 production plants powered by renewable electricity that can achieve high conversion and hydrogen product purity is thus an area of industrial interest. In a hydrogen plant, shift reactors, compressors, and heat exchange networks are needed to achieve better CH_4 conversion and higher H_2 production efficiencies. While these units cannot be practically implemented at experimental scales for purposes of process optimiza-

tion, they can be simulated using a process simulation software provided that the mathematical models for transport, reaction, and separation in the different units are experimentally validated.

In this work, a reformer model is built that is informed by experimental data generated by UCLA's electrically-heated steam methane reformer. This model is used within an Aspen simulation environment to simulate a scaled-up version of the plant with a hydrogen production capacity of 253 kg/h, which is closer to industrial production levels. The new Aspen Plus model includes a full plant model with shift reactors, and PSA for separation. Finally, a sensitivity analysis is carried out to determine the impact of key operating variables on the overall energy consumption and compare the conventional SMR process versus the electrified SMR process.

Chapter 2

Definition of Variables

- a: Specific outer surface area of the catalyst. $[\mathrm{m}^2 \cdot \mathrm{m}^{-3}]$
- $C_{\mathrm{CH_{4,\ inlet}}}$: Concentration of methane at the inlet of steam methane reformer. $[\mathrm{mol} \cdot \mathrm{m}^{-3}]$
- C_i: Concentration of species i. $[\mathrm{mol} \cdot \mathrm{m}^{-3}]$
- D_m: Molecular diffusivity. $[\mathrm{m}^2 \cdot \mathrm{s}^{-1}]$
- d_p: Adsorbent particle diameter. $[\mathrm{m}]$
- d_t: Diameter of the reactor. $[\mathrm{m}]$
- eff_{Energy}: Reformer energy conversion efficiency. [-]
- HHV_i: Higher heating value of gas species i. $[\mathrm{J/mol}]$
- k_G: Global mass transfer coefficient for a catalytic wall multichannel reactor. $[\mathrm{m} \cdot \mathrm{s}^{-1}]$
- K_i: Adsorption constant of gas species i. [Pa^{-1} for i = CH_4, H_2, CO and unitless for i = H_2O]

- K_j: Equilibrium constant for reaction j. [Pa^2 for j = 1 (SMR reaction), unitless for j = 2 (WGS reaction)]
- k_j: Reaction rate constant of reaction j. [$\mathrm{mol} \cdot \mathrm{Pa}^{0.5} \cdot (\mathrm{kg_{cat}} \cdot \mathrm{s})^{-1}$ for j = 1 (SMR reaction), $\mathrm{mol} \cdot \mathrm{Pa}^{-1} \cdot \mathrm{kg_{cat}}^{-1} \cdot \mathrm{s}^{-1}$ for j = 2 (WGS reaction)]
- k_m: Mass transfer coefficient. [$\mathrm{m} \cdot \mathrm{s}^{-1}$]
- L_t: Length of the reactor. [m]
- MTC_i: Mass transfer coefficient of species i. [$1/\mathrm{s}$ for $i = CH_4$, CO, CO_2, and H_2]
- $\dot{n}_{H_2,Out}$ and $\dot{n}_{H_2,In}$: Molar rate of hydrogen in the outlet and inlet of the reformer. [$\mathrm{mol/s}$]
- $\dot{n}_{CH_4,In}$: Molar rate of methane in the inlet of the reformer. [$\mathrm{mol/s}$]
- P_i: Partial pressure of gas species i. [Pa]
- ρ_g: Density of the gas species i in the reactor. [$\mathrm{kg} \cdot \mathrm{m}^{-3}$]
- r_{net}: Net reaction rate for the steam methane reformer. [$\mathrm{mol} \cdot \mathrm{kg}^{-1} \cdot \mathrm{s}^{-1}$]
- r_1^{SMR}, r_2^{WGS} and r_2^{HT-WGS}, r_2^{LT-WGS}: Rates of steam methane reforming reaction, water gas shift reaction in the reformer, the high-temperature shift reactor and the low-temperature shift reactor. [$\mathrm{mol} \cdot \mathrm{kg}^{-1} \cdot \mathrm{s}^{-1}$]
- T: Reactor temperature. [K]
- t_m: Characteristic mass transfer time. [s]
- t_r: Characteristic reaction time. [s]
- u: Linear velocity through the reactor. [$\mathrm{m} \cdot \mathrm{s}^{-1}$]
- v_g: Fluid superficial velocity. [$\mathrm{m} \cdot \mathrm{s}^{-1}$]

Chapter 3

Modeling of Electrified Steam Methane Reforming Process via Aspen

The objective of the first part of this work is to simulate the electrically-heated steam methane reforming-based H_2 production plant using process simulators to examine the impact of key process parameters. In this process, H_2 is produced by the reaction of methane and steam flow to the reactor, as shown in Eq. 3.1, which presents the steam methane reforming reaction (Eq. 3.1a) and the water gas shift (WGS) reaction (Eq. 3.1b):

$$\text{Steam methane reforming} : \text{CH}_4 + \text{H}_2\text{O} \rightleftharpoons 3\text{H}_2 + \text{CO}, \quad \Delta H_{298} = 206.1\ kJ \cdot mol^{-1} \tag{3.1a}$$

$$\text{Water gas shift} : \text{CO} + \text{H}_2\text{O} \rightleftharpoons \text{CO}_2 + \text{H}_2, \quad \Delta H_{298} = -41.15\ kJ \cdot mol^{-1} \tag{3.1b}$$

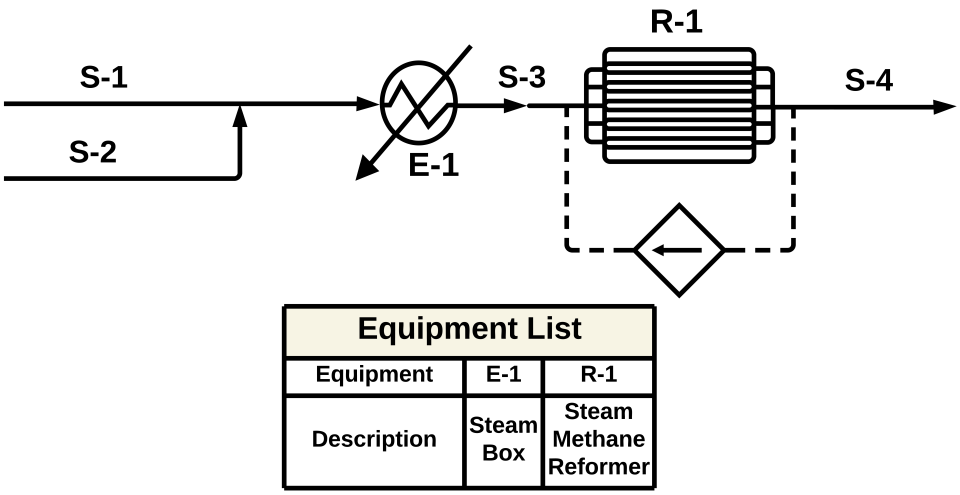

Figure 3.1: Aspen Plus reformer model emulating the Joule-heated experimental setup.

3.1 Process Overview

The proposed steam methane reforming-based H_2 production plant is simulated using Aspen Plus V12 and is in accordance with the process proposed in Reference [11]. The simulation can be divided into three main sections which are the electrified steam methane reforming (e-SMR) process, water gas shift reactors, and the pressure swing adsorption section. The operational parameters for the sections have been defined in Table 3.1. The e-SMR is simulated as a plug flow reactor using the $RPLUG$ reactor block. The CH_4 stream is compressed using a three-stage compressor with an intercooling temperature ratio of 0.85. All stages are set to the same pressure ratio and compressed CH_4 is mixed with steam. The e-SMR is assumed to run on electricity derived from renewable sources, which further reduces upstream CO_2 emissions.

For the reformer section of the overall process simulation (see Fig. 3.1), heat transfer must be accounted down the length of the reformer since the SMR reactions generate and consume varying amounts of heat at different axial positions. Thus, the reforming unit needs the correct energy information to adequately model the composition and kinetic profiles along the length of the reformer,

Table 3.1: Operational parameters for industrial-scale H_2 production process simulation in Aspen V12.

Process	Description
SMR	Plug flow reactor with Ni/ZrO_2 washcoated catalyst. Operating conditions: 868–1028 °C, 16 bar Length: 4.57 m Diameter: 0.0099 m Number of tubes: 774 Catalyst weight: 15 kg $r_1^{\text{SMR}} = \frac{k_1^{\text{SMR}}}{P_{\text{H}_2}^{2.5}} \frac{P_{\text{CH}_4}P_{\text{H}_2\text{O}} - P_{\text{H}_2}^3 P_{\text{CO}}/K_{\text{eq},1}^{\text{SMR}}}{(1 + K_{\text{CO}}P_{\text{CO}} + K_{\text{H}_2}P_{\text{H}_2} + K_{\text{CH}_4}P_{\text{CH}_4} + K_{\text{H}_2\text{O}}P_{\text{H}_2\text{O}}/P_{\text{H}_2})^2}$ $r_2^{\text{WGS}} = \frac{k_1^{\text{WGS}}}{P_{\text{H}_2}} \frac{P_{\text{CO}}P_{\text{H}_2\text{O}} - P_{\text{H}_2}P_{\text{CO}_2}/K_{\text{eq},1}^{\text{WGS}}}{(1 + K_{\text{CO}}P_{\text{CO}} + K_{\text{H}_2}P_{\text{H}_2} + K_{\text{CH}_4}P_{\text{CH}_4} + K_{\text{H}_2\text{O}}P_{\text{H}_2\text{O}}/P_{\text{H}_2})^2}$
HT-WGS	Plug flow fixed bed reactor contains a Fe_2O_3/Cr_2O_3/CuO based catalyst. Operating conditions: 449-543 °C, 15.8 bar Packed bed length: 1.58 m Packed bed diameter: 0.79 m Catalyst weight: 500 kg $r_2^{\text{HT-WGS}} = 10^{5.854} \exp \frac{-1.11 \times 10^5 \pm 2.63}{RT} P_{CO}^{1.0} P_{CO_2}^{-0.36} P_{H_2}^{-0.09} (1 - \frac{1}{K_2} \frac{P_{CO}P_{H_2}}{P_{CO}P_{H_2O}})$
LT-WGS	Plug flow fixed bed reactor contains a Cu/ZnO/Al_2O_3 based catalyst. Operating conditions: 251-274 °C, 15.2 bar Packed bed length: 1.42 m Packed bed diameter: 0.71 m Catalyst weight: 100 kg $r_2^{\text{LT-WGS}} = 1.329 \exp \frac{-34.983 \times 10^3}{RT} P_{CO}^{0.854} P_{H_2O}^{1.99} P_{H_2}^{-1.926} P_{CO_2}^{-0.573} (1 - \frac{1}{K_2} \frac{P_{H_2}P_{CO_2}}{P_{CO}P_{H_2O}})$

and this work discusses two different approaches to energy modeling in the reformer section of the simulation. The first approach is explained in this section and involves programming a heat flux

profile down the length of the reactor to match the experimental thermocouple measurements in the same positions (13.5 cm and 34.25 cm from the outlet of the reformer). Given that the experiments only have two thermocouples, the experimental energy information is limited, and the heat flux profiles that are programmed into Aspen are approximations of the true energy distribution. The programmed heat flux profiles are not unique and can be programmed in a variety of ways. The lab-scale simulation in Fig. 3.1 contains discrete-valued flux profiles that make physical sense under the notion that the endothermic reforming reaction requires a significant heat of reaction at the beginning of the reformer tube. The second approach, discussed in Section 3.2, selects an average heat flux for the entire reactor that provides the desired steady-state temperature at the outlet of the reformer. The second approach is needed for the SMR scale-up procedure to be discussed below because the temperature and flux profiles for an electrically heated, washcoated reformer at elevated pressures and space velocities are experimentally unknown. To our knowledge, this is the first experimentally validated Aspen model for a Joule-heated reformer with a Ni/ZrO_2 washcoated catalyst at 1 bar and 5 bar.

The reformer section focuses on H_2 production according to Eq. 3.1a, while the shift reactor section aims to convert the CO products generated by the reformer section, as per Eq. 3.1b. The WGS reaction is exothermic, so it is favored at lower temperatures compared to the net endothermic reforming reactions. Hence, in order to convert the remaining CO into CO_2 to create more H_2, shift reactions take place at lowered temperatures. In the shift reactors, different catalysts are employed for the high-temperature and low-temperature WGS (LT-WGS) reaction. The operational conditions for these shift reactors are defined according to Reference [12]. For the high-temperature WGS (HT-WGS), an adiabatic reactor using a $RPLUG$ block is chosen and the Fe-Cr commercial catalyst is used. Based on Reference [13], the rate equation in Table 3.1 ($r_2^{\text{HT-WGS}}$) is used to simulate the HT-WGS catalytic reaction rate with the Fe-Cr commercial catalyst. For the low-temperature WGS, a second adiabatic $RPLUG$ reactor block is chosen and based on Reference [14], the rate equation in Table 3.1 ($r_2^{\text{LT-WGS}}$) is used to simulate the LT-WGS catalytic

reaction rate with the $CuO/ZnO/Al_2O_3$ commercial catalyst. The sizing of the shift reactors was based on the criteria set fourth in Reference [15] in their reactor design case study that suggests a 4.5 s residence time for each shift reactor and a length-to diameter ratio of about 2:1. Per this instruction, the shift reactors' packed beds are 1.58 m and 1.42 m long with outer diameters of 0.79 m and 0.71 m for the HT-WGS reactor and the LT-WGS reactor, respectively. The residence times of the shift reactors are 4.3 s and 4.5 s for HT-WGS and LT-WGS reactors, respectively, and the effluent gas from the HT-WGS and LT-WGS section is subsequently purified. The main molecules that need to be removed from this effluent stream are steam and CO_2. Steam removal is achieved through a condenser, as steam can be liquefied at lower temperatures, and any remaining water is removed through a molecular sieve dryer. The dryer mitigates the influence of water content on the PSA unit as molecular sieve adsorption beds with zeolite 3A can absorb residual process water. The water-holding capacity of a 3A molecular sieve zeolite is typically 20% of the weight of the sieve. In addition, Reference [16] implied that the water adsorption bed is regenerated after 12-36 h of adsorption in industrial settings. In this study, two adsorption beds, each containing 675 kg of a 3A zeolite molecular sieve, are utilized. One bed operates for 24 h to remove water from the stream. Once this bed becomes saturated with water, it undergoes regeneration, while the stream is diverted to the other bed to continue the adsorption process. The subsequent stream is sent to the PSA section for purification. The final outlet stream of the overall process contains 99% pure hydrogen. The gas stream leaving the dryer is mainly composed of H_2 and CO_2. Subsequently, CO_2 removal is accomplished via the PSA process, from which the effluent yields high-quality H_2 production with 99% purity.

3.2 Aspen Plug Flow Reformer Model Comparison to Experimental Results

The Aspen reformer process faithfully models the experimental setup (Fig. 3.1), using the same dimensions, inlet flowrates for each gas (including Argon which is used as a tracer in the experimental setup), catalyst weight, and temperatures. The experimental setup employs two K-type thermocouples located on the reactor wall of the inlet section and of the outlet section. The experimental temperatures were recorded from both thermocouples and used as input to the $RPLUG$ reactor to represent the tube inlet and outlet temperatures. The production rates are described in standard cubic centimeters per minute (sccm).

The experimental electrified SMR process contains a series of mass flow controllers that modulate and maintain the inlet flow streams of CH_4, H_2, and Ar (39.4/17.7/6.5 sccm). The dry gas inlet mixture travels through a bubbler where it is mixed with water vapor in a 3:1 S/C ratio. To generate the appropriate steam flowrate to achieve this ratio, a Watlow PI controller regulates the energy input to the heating tape that surrounds the stainless steel bubbler casing. The temperature setpoints of the gas bubbler to produce a 70 % steam inlet mixture, or 119.5 sccm, are 96 °C at 1 bar and 144 °C at 5 bar. The bubbler efficiencies are known to be around 94% so the temperature setpoint is slightly higher than the theoretical setpoint. After the dry gas stream is mixed with water vapor at the desired S/C ratio, the stream is heated to 150 °C. The mixture proceeds to the reformer built from a 5.4 mm diameter and 500 mm length Goodfellows FeCrAlloy © tube where the gasses come into contact with Ni surface sites on a ZrO_2 washcoat. The Ni loading in the reformer is 158.0 mg which is also the catalyst weight used for computational modeling. The reformer effluent flows through a stainless-steel shell casing, cooled by ambient temperature water. The cooled, unreacted water vapor liquefies and collects in condenser bottles. The remaining gas product mixture flows through an automated gas chromatograph (GC), and the mixture components are quantified before venting.

To validate the Aspen Plus electrified reformer simulation model, steady-state data collection occurred at 1 bar and 5 bar system pressures over the outlet temperature range of 500 to 800 °C. A theoretical heat flux profile is provided as an input to the experimental-scale Aspen reformer model to adequately describe energy consumption and generation driven by the SMR and WGS reactions over the length of the reactor. The heat flux parameters of the Aspen plug flow reformer model were adjusted to mirror the experimental thermocouple measurements at 34.25 cm and 13.5 cm from the reactor outlet. The heat flux configurations with temperature and CH_4 conversion results are provided in Fig. 3.2. Specifically, the heating profiles programmed in Aspen are shown in Fig. 3.2a and Fig. 3.2b. The initial heat flux consumed by the SMR reactions is higher for the first 40% of the tube length, where the endothermic reaction dominates. For the remainder of the tube length, the WGS reaction dominates, providing exothermic heat to the reformer and lessening the energy flux requirement. This behavior is the same for all reformer simulations, and the inlet heat flux requirements range from 0.662 $\mathrm{kW/m^2}$ to 3.11 $\mathrm{kW/m^2}$ under the different system pressures. Given additional axial temperature measurements, the programmed flux profile would gain accuracy and become increasingly linear as was seen in the e-SMR experiments conducted in Reference [17]. It is also thought that the resulting temperature profiles, seen in Fig. 3.2c and Fig. 3.2d, would become increasingly linear as well. Still, the programmed heating profiles provide a good estimate of the average energy requirements over the entire length of the reactor as evidenced by the general agreement between the experimental and computational gas product molar flowrates in Fig. 3.3 and Fig. 3.4. Further, the conversion profiles at both pressures, being aligned with the position-dependent temperature measurements, reveals most methane conversion occurs in the first 50% of the reactor length, with much less conversion occurring in the second 50%. The only exception to this trend occurs for the 479.6 °C steady-state at 1 bar and the 463.3 °C steady-state at 5 bar. At lower temperatures, the conversion is lower, and thus the heat flux is more homogeneous along the length of the reactor.

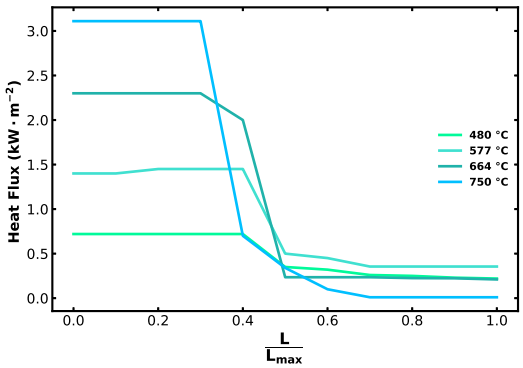

(a) Steady-state heat flux profile at 1 bar.

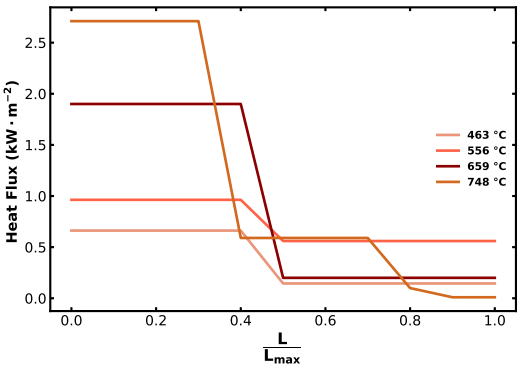

(b) Steady-state heat flux profile at 5 bar.

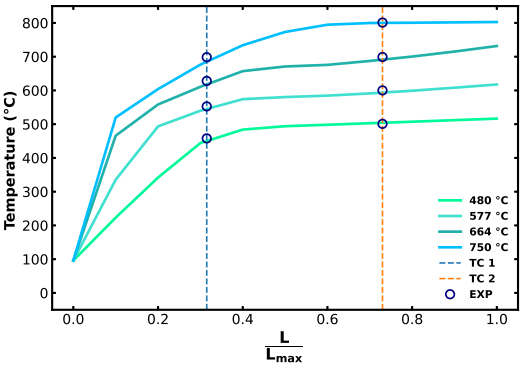

(c) Steady-state temperature profile at 1 bar.

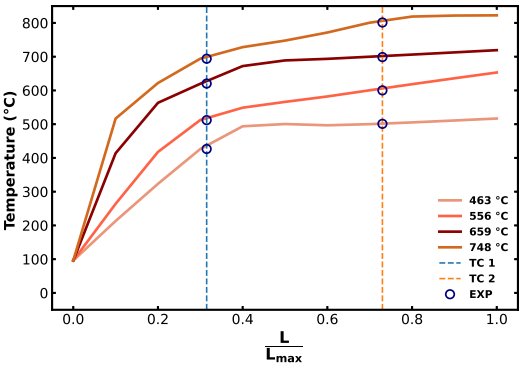

(d) Steady-state temperature profile at 5 bar.

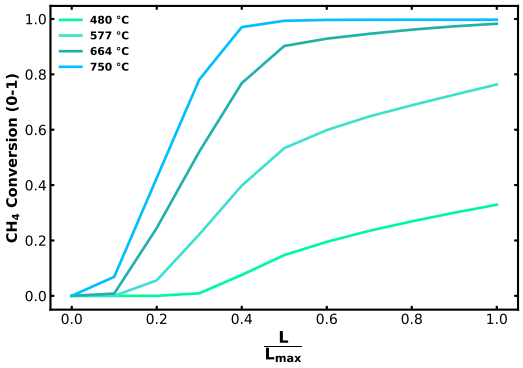

(e) CH_4 conversion profile at 1 bar.

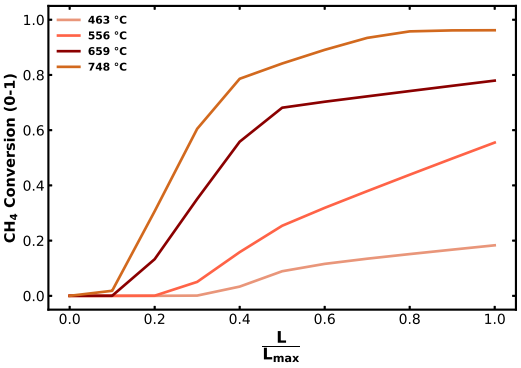

(f) CH_4 conversion profile at 5 bar.

Figure 3.2: Aspen plug flow reforming reactor simulation; heat flux configuration with temperature and conversion results as a function of the reformer length.

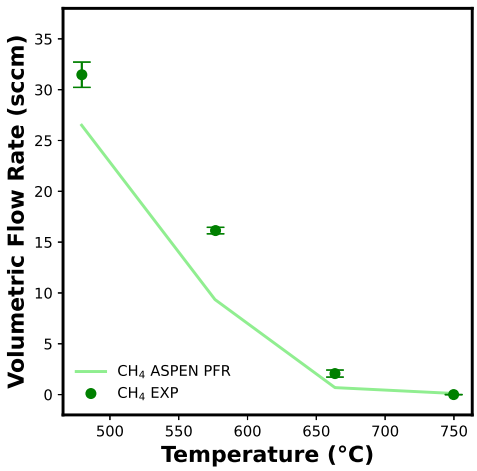

(a) CH_4.

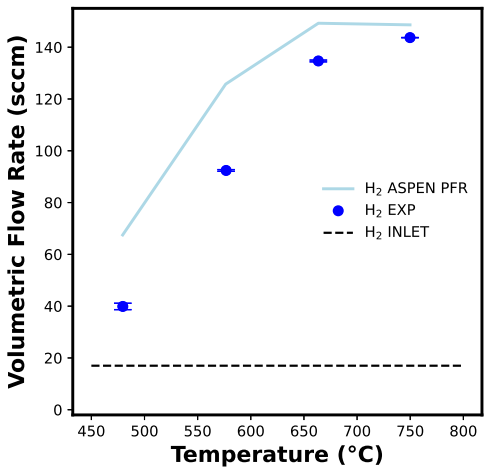

(b) H_2.

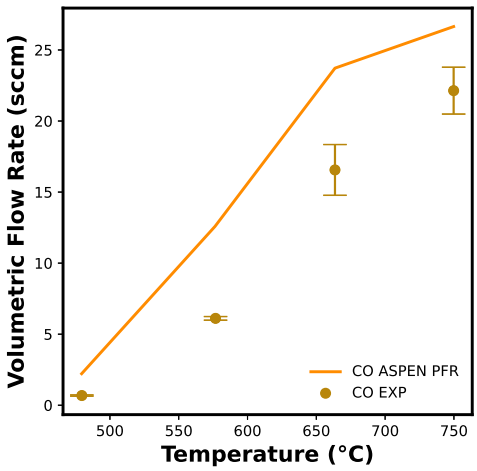

(c) CO.

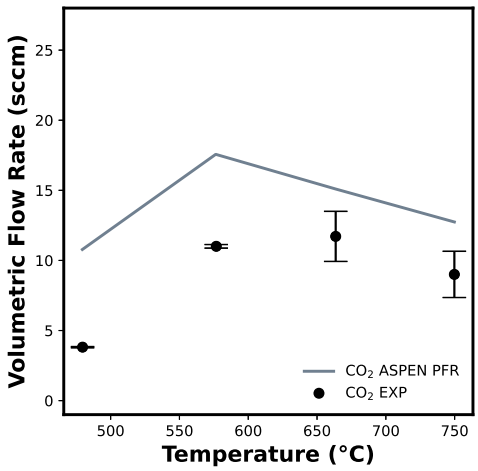

(d) CO_2.

Figure 3.3: Joule-heated experimental gas product stream comparison to the Aspen Plus SMR reactor model at 1 bar. The error bars represent the standard deviations of steady-state GC measurements.

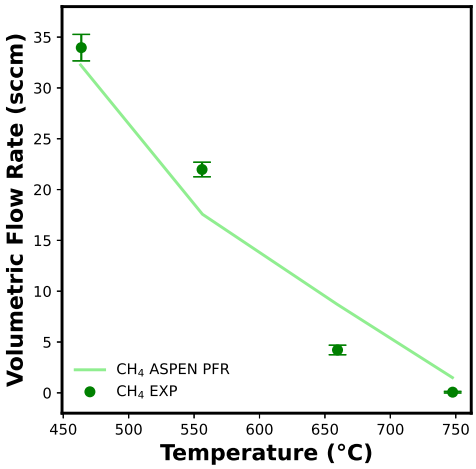

(a) CH_4.

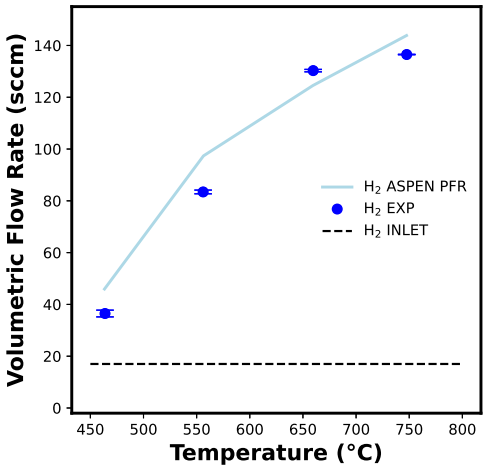

(b) H_2.

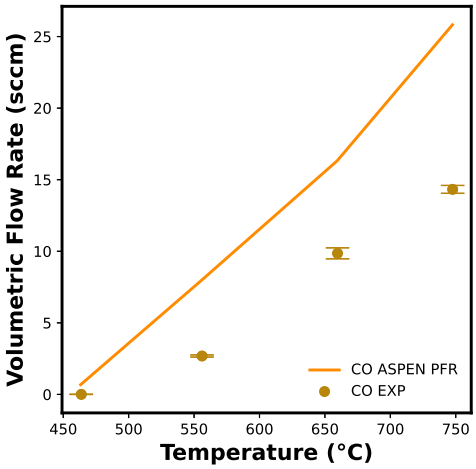

(c) CO.

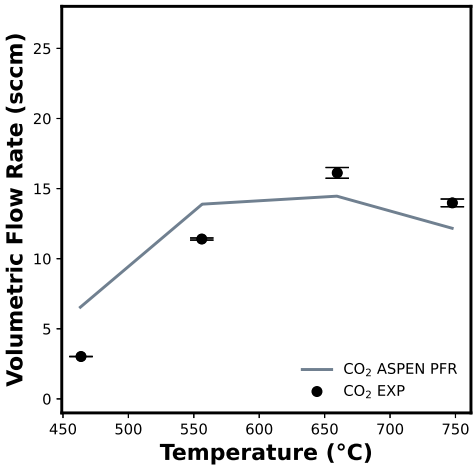

(d) CO_2.

Figure 3.4: Joule-heated experimental gas product stream comparison to the Aspen Plus reformer model at 5 bar. The error bars represent the standard deviations of steady-state GC measurements.

Temperature control over the experimental reformer to ramp and maintain the outer wall temperature of the tube is provided in detail in References [9] and [8, 10]. Experimental results were expected to follow the conversion trends of the Aspen PFR computational model with changes in temperature and pressure. However, considering molecular dissociations into carbon atoms by CH_4 thermal decomposition [18], the Boudouard, and CO disproportionation [19] reactions at higher steady-state temperatures, larger absolute errors between Aspen-predicted and experimentally-measured CO and CO_2 flowrates were also anticipated (Fig. 3.5). Rates of carbon formation (coking) tend to increase with temperature, and carbon formation peaked at 5 bar and 747.5 °C assuming all losses to the carbon balance, in sccm units, result from missing CH_4 that has turned into solid carbon. Experimental heat losses are documented in Fig. 3.5a which shows the average external heat loss from the reformer's outer wall into the surroundings. It is also thought that the packed bed kinetic model, adopted from Reference [20], differs from the Ni/ZrO_2 washcoat kinetics. The over-prediction of the Aspen PFR model in Fig. 3.2c is thought to reflect the physical geometric difference between the packed bed and washcoat and the impact of catalyst geometries on bulk mass transfer to Ni active sites. Additionally, the fraction of the total energy that is not consumed by the internal reforming reactions is reported. External heat losses range from 5.95 to 13.62 $\mathrm{kW/m^2}$ and increase with the steady-state temperature of the reformer. The fractional heat losses, dependent on methane conversion, range from 90.7% to 94.4% and are minimized at 556.4 °C under 5 bar conditions. With over 90% of energy losses to ambient surroundings, this novel process stands to gain the most percentage points in energy conversion efficiency from improvements to the thermal insulation layer encapsulating the reformer. Root-mean-squared-error (RMSE) values were used to establish the performance of the 1 bar and 5 bar Aspen PFR steady-state simulations. At 1 bar, the errors for CH_4, H_2, CO, and CO_2 were 4.26, 22.97, 5.38, and 5.41, respectively. It is thought that the hydrogen error was exacerbated by lower mass transfer to Ni surface sites on the washcoat at lower pressures or by the inhibition of active catalytic sites due to carbon formation. It may also be possible that the larger error in H_2 measurements is a byproduct

of the larger magnitude of the hydrogen flowrate in comparison to the other gas product species. Further, GC measurement errors range from 1-5% and contribute to the model error as well. The RMSE values for the 5 bar steady-state measurements and CH_4, H_2, CO, and CO_2 predictions were 3.34, 9.62, 7.12, and 2.48, respectively. Most notably, the gas product trends align with the Aspen models, providing an experimental validation for high-pressure process intensification.

Reformer conversion efficiencies were calculated using Eq. 3.2:

$$eff_{\text{Energy}} = \frac{(\dot{n}_{\text{H}_2,\text{ Out}} - \dot{n}_{\text{H}_2,\text{ In}}) \times HHV_{\text{H}_2}}{\dot{n}_{\text{CH}_4,\text{ In}} \times HHV_{\text{CH}_4} + Average\ Power\ Input} \times 100\% \tag{3.2}$$

where the reformer energy conversion efficiency is equal to the molar flowrate of hydrogen produced times the higher heating value (HHV) of hydrogen gas divided by the quantity that multiplies the molar flowrate of inlet methane with its HHV and adds the average power input from the DC power supply. This calculation is formulated as such to provide a ratio of the output energy stored in the chemical bonds of the H_2 target product to the input energy in the form of resistance heating and chemical energy stored in CH_4 molecules. The optimal energy conversion efficiencies for the 1 bar and 5 bar experiments were achieved at the 663.6 °C and 659.4 °C steady-state temperatures, which are calculated using an arithmetic average of the top and bottom thermocouple values. Fig. 3.6 shows a 20.2% energy conversion efficiency at 1 bar which increases to 22.7% around the same temperature at 5 bar. In the Aspen simulation, optimal energy conversion efficiencies occur at the 749.8 °C and 747.5 °C steady-state temperatures. The energy efficiency of the 1 bar simulation at the aforementioned temperature is 83.2% which exceeds the optimal efficiency of the 5 bar simulation by 2.0%. Considering the Aspen model is not equipped to account for external heat losses to the surroundings, the simulation energy efficiencies are about four times that of the experiments at either system pressure. The average heat loss to the surrounding environment is provided in Fig. 3.5a. In the future, experimental energy losses can be minimized by providing better thermal insulation to the reformer tube and to the upstream and downstream pipelines.

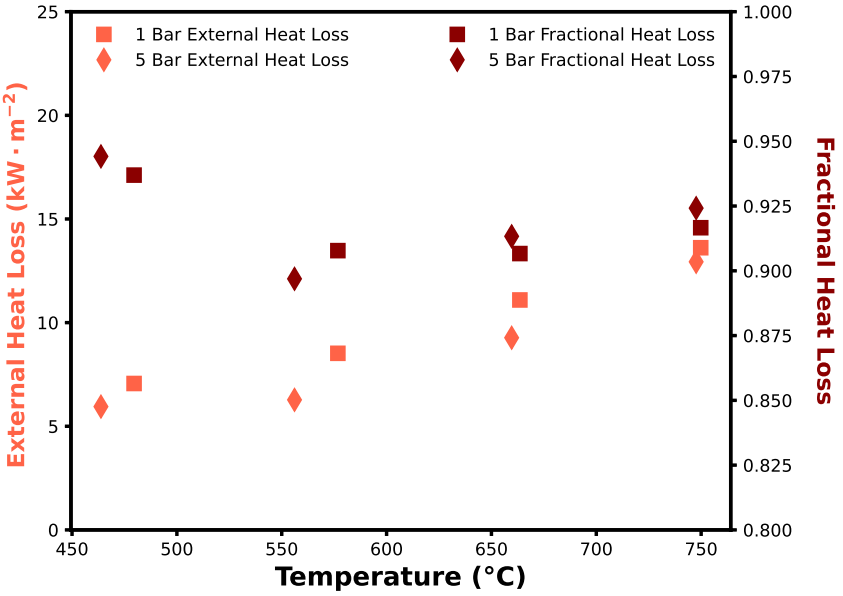

(a) Experimental external heat flux to the surroundings (heat losses that are not kinetically consumed).

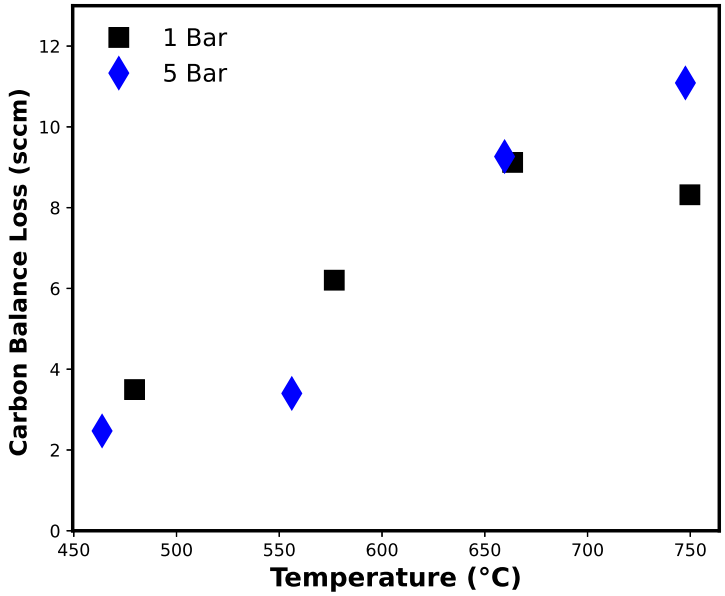

(b) Experimental carbon balance error introduced by varying levels of solid carbon formation.

Figure 3.5: Experimental heat energy and carbon balance losses at 1 bar and 5 bar for 463 to 750 °C steady-state temperatures.

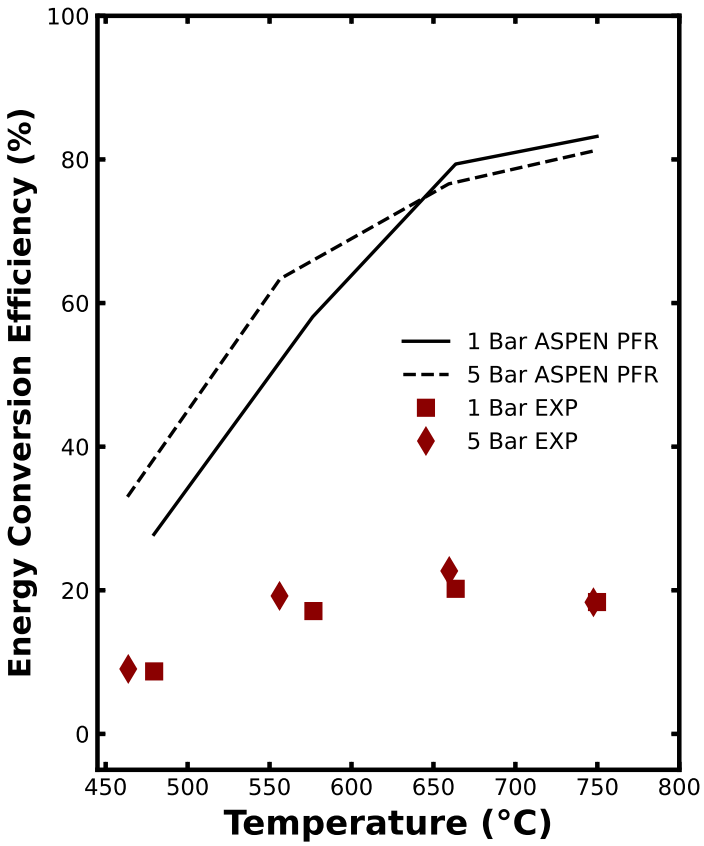

Figure 3.6: Aspen Plus $RPLUG$ electric reformer model (Fig. 3.1) and experimental energy conversion efficiencies (Eq. 3.2) as a function of temperature and pressure.

It must also be added that some of the power input to the experimental system goes into heating the insulation layers and surrounding metals. As a consequence, there is a large inertial mass that is heated as the experimental bench setup is operated at higher temperatures. These heat losses will be minimized in industrial electrified reformers.

The scale-up of the process was done using dimensionless variables approach and is discussed in detail in Reference [21]

3.3 SMR Flowsheet Overview

The scaled-up version of the SMR simulation, referred to here and throughout the rest of this study, incorporates essential unit operations and adjusts the process inlet parameters according to prior experimental findings. The configuration of the reactors is mentioned in Table 3.1. At the beginning of the flowsheet, pressurizing methane and steam is essential for operating at industrial because of equipment sizing constraints. Increasing the pressure also helps to maintain the GHSV of 1000 h^{-1} from the experimental setup. The methane stream undergoes pressurization through a multistage compressor, which consists of 3 stages with an equal pressure ratio of 2.51 and inter-coolers that are specified such that the ratio of outlet temperatures to inlet temperatures at every stage is 0.85. The simulation gives better energy conversion and total system efficiencies at lower pressures; however, this would lead to impractical reformer tube diameters for the same space velocity. The multistage compressor is followed by the mixing of methane with the preheated steam using a mixer. The water stream is at a temperature of 201 °C which is essential for maintaining a S/C ratio of 3 at the operating pressure. This mixed stream is fed into the steam methane reformer and the outlet temperature for the reformer varies from 868 to 1028 °C depending on the chosen heat flux values. The compressed, wet reactant stream undergoes the steam methane reforming reaction (Eq. 3.1a) and (Eq. 3.1b) in the presence of the Ni/ZrO_2 catalyst, following the kinetics described by [20]. Subsequently, the stream is cooled and is fed into the high-temperature water gas shift reactor, HT-WGS as seen in Fig. 3.7. The stream undergoes catalytic reaction at 449 °C with the reaction rate ($r_2^{\text{HT-WGS}}$ in Table 3.1). Afterward, the cooled product stream of the HT-WGS reactor feeds into the low-temperature water gas shift reactor and undergoes the water gas shift reaction at 252 °C with reaction rate ($r_2^{\text{LT-WGS}}$ in Table 3.1). Thereafter, the product stream is brought to 25 °C and then flashed. The condensed water is removed through the bottoms and the vapor containing hydrogen is sent to the molecular sieve water removal section to eliminate the remaining water as seen in Fig. 3.8. Finally, the vapor-containing stream is sent all the way

downstream to PSA section for the recovery of high-purity hydrogen product.

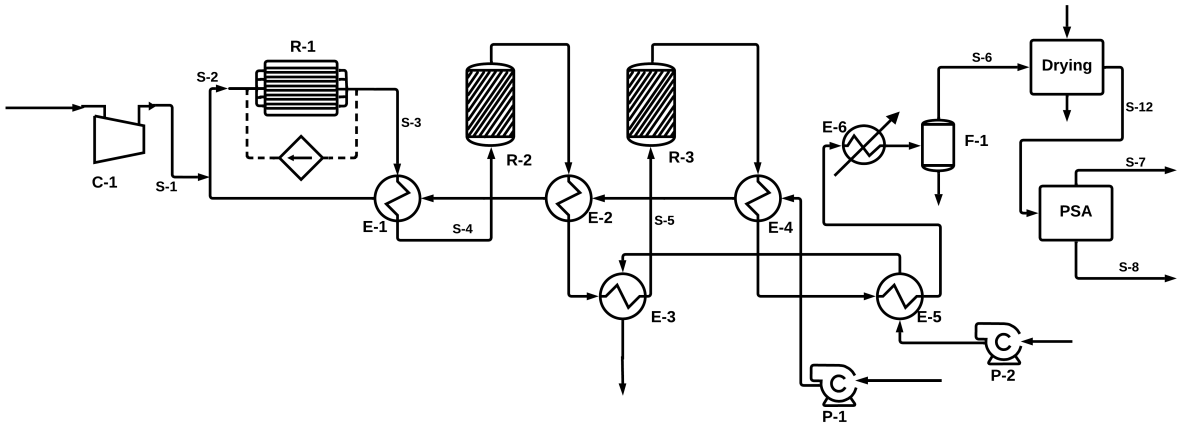

Equipment List														
Equipment	C-1	R-1	R-2	R-3	E-1	E-2	E-3	E-4	E-5	E-6	P-1	P-2	F-1	V-1
Description	Multistage Compressor with Intercoolers	SMR Reactor	HT-WGS Reactor	LT-WGS Reactor	SMR Product Heat Exchanger	HT-WGS Product Heat Exchanger	LT-WGS Feed Heat Exchanger	LT-WGS Product Heat Exchanger	LT-WGS Product Heat Exchanger	Pre-Flash Cooler	Process Water Pump	Cooling Water pump	Flash Drum	Valve

Figure 3.7: Optimized flowsheet of the overall SMR process comprised of an electric reformer, two WGS reactors, heat integration, raw gas cooling and drying units, and pressure swing adsorption. Comprehensive process flow diagram for the Drying block provided in Fig. 3.8. This process also generates 363 kg/h of saturated steam (204.5 °C and 1.7 MPa).

Table 3.2: SMR overall process simulation stream conditions and compositions for streams 1-8.

Stream no.	1	2	3	4	5	6	7	8
Mole flows (%)								
CH_4	69.3	22.4	0.4	0.4	0.4	0.5	1.9	0
H_2O	0	67.7	28.4	28.4	20.1	0.2	0.9	0
H_2	30.7	9.9	56	56	64.3	80.8	29	99.4
CO	0	0	11.6	11.6	3.3	1.2	3.7	0.4
CO_2	0	0	3.6	3.6	11.9	17.2	64.5	0.2
Temperature ($°C$)	25	260	978	507	252	25	14	29
Pressure (kPa)	800	1700	1600	1580	1520	1380	250	1380
Mass flows (kg/h)	503	2121	2121	2121	2121	1516	1263	253

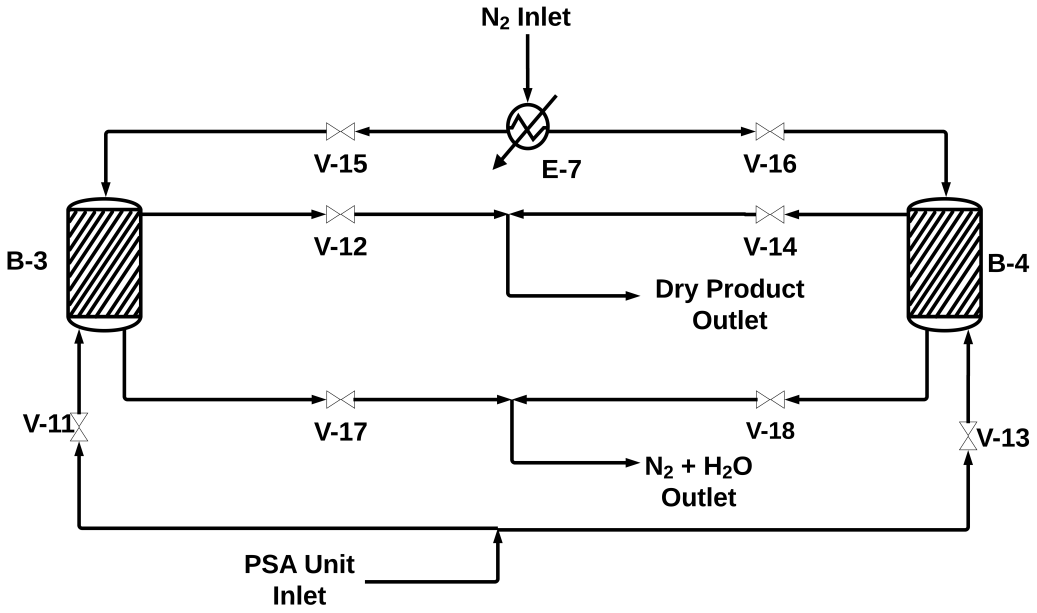

Equipment List											
Equipment	B-3	B-4	V-11	V-12	V-13	V-14	V-15	V-16	V-17	V-18	E-7
Description	Molecular Sieve Dryer 1	Molecular Sieve Dryer 2	Feed Valve for Dryer 1	Product Valve for Dryer 1	Feed Valve for Dryer 2	Product Valve for Dryer 2	Purge Inlet Valve for Dryer 1	Purge Inlet Valve for Dryer 2	Purge Outlet Valve for Dryer 1	Purge Outlet Valve for Dryer 2	Heater for Purge

Figure 3.8: Molecular sieve dryer process flow diagram.

Chapter 4

Flowsheet Optimization

4.1 Heat Integration

The optimization of the flowsheet consisted of two parts. The first part included replacing the heaters and coolers with a dedicated network of heat exchangers to perform heat integration and minimize the potential of any lost duty through heat recovery. Since the outlet temperature of the reformer is significantly high, it can be used to create the pressurized steam feed. Similarly, a network of heat exchangers lowers the temperature of the reformer effluent before it is sent to the shift reactors. The model fidelity of the exchangers in the Aspen Plus simulation is set to "Shortcut" and they are maintained at a hot/cold minimum approach of 50 °C with the flow direction set to countercurrent. Four heat exchangers and two coolers lower the temperature of the process gas from 978 to 25 °C. The total recovered duty from the heat integration network is 1.6 MW, excluding a utility loss of 0.7 MW. Through this method, a significant portion of the heat is recovered and utilized for steam generation.

4.2 Parametric Study: Electrified SMR Process

The second part of optimization involved making minor adjustments to the geometries of the units and H_2 production rates to achieve a flow rate of 253 kg/h with 99% H_2 purity. To speed up this process, a Python script was developed to connect to the Aspen Plus simulation using the Aspen Plus application programming interface (API). The API is typically accessed through the 'win32com' library, which allows Python to interact with COM (Component Object Model) objects. This enables backend control over the Aspen Plus simulations to run tasks and to extract desired data in an efficient manner. This facilitates the testing of various scenarios with different inputs and operational parameters without manually changing the simulation flowsheet. This proves to be a faster method than performing sensitivity analysis using the in-built Aspen tools, as the Python script allows the varying of multiple input and operational parameters at the same time. The data values from the Aspen simulation are extracted using the "Variable Explorer," and once the correct node for the desired parameter is identified, it can be modified using the script by calling onto that node. The above method is used to vary the configurations of the plug flow reactors, reaction conditions, catalyst weight, number of tubes, tube length, and tube diameter. As seen in Fig. 4.1, a parametric study is performed by varying the pressure in the reformer system and comparing the SMR efficiencies and methane conversion values for different average fluxes along the length of the reformer (26-32 $\mathrm{kW/m^2}$).

The efficiencies were calculated using Eq. 3.2 with the average power input being derived from the total duty of the reformer for the energy conversion efficiency. For the total efficiency of the entire system, duties of the reformer along with the energy requirements for the pumps, multistage compressor, cooler, molecular sieve dryers, and the PSA section were taken into account. The conversion efficiency decreases with an increase in pressure, which can be attributed to lower methane conversion, and consequently, lower hydrogen production at elevated pressures. However, a higher pressure is necessary to maintain a suitable space velocity near 1000 $\mathrm{h^{-1}}$, a linear

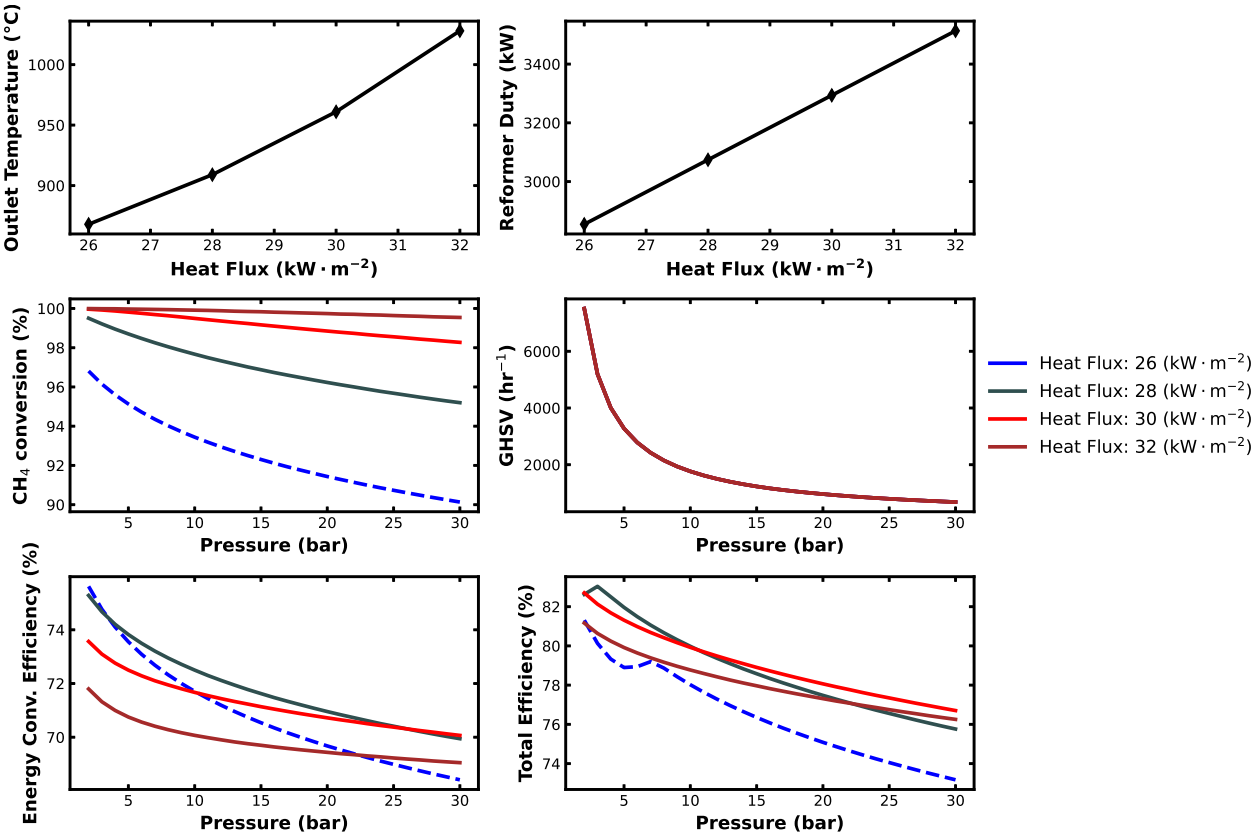

Figure 4.1: Parametric study on industrial-scale Aspen simulation containing a multitube reformer with adiabatic outer walls. The sensitivity analysis explores the simulation response to a variable reformer heat flux (26-32 $\mathrm{kW/m^2}$) and variable system pressure (1-30 bar). Dashed lines indicate nonviable system configurations. Solid lines indicate practical system configurations.

velocity below 1.5 m/s, and a viable sizing of the reformer. For each heat flux, as the pressure of the system is modulated, the overall reformer duty is unchanged which indicates that the reformer duty is only a function of the flux. The parameter values mentioned in Table 3.1 were obtained after performing the given analysis and taking into account economic and practical operation limits. It was determined that the most optimal case would be a pressure of 16 bar and average heat flux around 30 $\mathrm{kW/m^2}$ which results in an outlet temperature near 960 °C and a total efficiency of 78%. This specific outlet temperature is selected because of the washcoated-Ni/ZrO_2 catalyst undergoes unsustainable deactivation and sintering at temperatures above 1000 °C which imposes operational limits on such processes [22]. Additionally, e-SMR is a novel process with undeter-

mined industrial-scale energy losses. The experimental setup discussed in Section 3.2 experiences approximately 90% heat loss to the lab environment (Fig. 3.5a), however, the setup is not optimized to be thermally insulating. The reality is that electrical reforming avoids generating excess CO_2 during heating and will gain overall process efficiency with the advent of thermally insular materials with geometries suited for multitube reformers. Assuming only electrical energy inputs from non-fossil fuels, the optimal SMR and PSA Aspen model generates 5.08 kg CO_2-eq/kg H_2. This e-SMR design has the potential to decrease SMR emissions by 46% when compared to today's best available SMR technology, without carbon capture, which produces 9.00 kg CO_2-eq/kg H_2 according to Reference [23].

4.3 Comparative Energy & Emissions Analysis: Conventional vs. Electrified SMR Process

The traditional route to hydrogen production by way of steam methane reforming is known as the conventional SMR process. The conventional process is equipped with a combustion furnace that burns natural gas to supply thermal energy to the reactor coils of the reformer unit and to chemically convert natural gas into a value-added hydrogen product. The motivation for at-scale electrified reforming processes that utilize renewable electricity is highlighted in the comparison of carbon emissions from the conventional and electrified process simulations. A conventional SMR process scheme was simulated in Aveva's PRO/II software in Reference [21], with the simulation providing the required inputs, unit operations, and overall energy conversion to maintain the same 253 kg/h H_2 production capacity from the electrified process design.

Heat integration in the conventional SMR process has additional complexities due to the availability of recoverable energy in the flue gas stream that exits the furnace and originates from the combustion of CH_4 at 1200 °C. A total of eight heat exchangers and two coolers are used for the PRO/II simulation as discussed in Reference [21], and the temperature of the flue gas stream is

decreased from 1200 to 200 °C by transferring thermal energy to the high pressure steam feed for reforming, the process gas feed for pre-reforming, and the compressed air feed. The post-reformer effluent is also used to generate high pressure steam. Overall, 5.1 MW of thermal energy is recovered from heat exchange network and 0.8 MW is lost through cooling utilities. Though the conventional heat exchanger network recovers a larger amount of heat, the electrified system loses 0.7 MW to cooling utilities (Fig. 4.2). The electrified system also requires half the number of heat exchanger units which helps to lower the additional capital cost incurred from the need for a LT-WGS reactor. Two Sankey diagrams in Fig. 4.3 map the energy inputs of both process designs to their respective energy outputs. The natural gas feed requirement is 19.9 GJ/h greater for the conventional reforming design to fuel its distinctive combustion reaction, and an additional 6.4 GJ/h input is needed overall for this classical reforming scenario. The electrified reforming design produces more H_2 product and has fewer thermal losses when compared to the conventional design under similar conditions. Another distinction between the two reformation models, from an energy standpoint, is the lack of a PSA off-gas recycle for the e-SMR design, understanding that the electrified process does not have a furnace to which off-gas can be burned. Still, both designs have similar energy utilization and loss, so the primary justification for an electrified reforming system lies in its potential to significantly reduce carbon emissions.

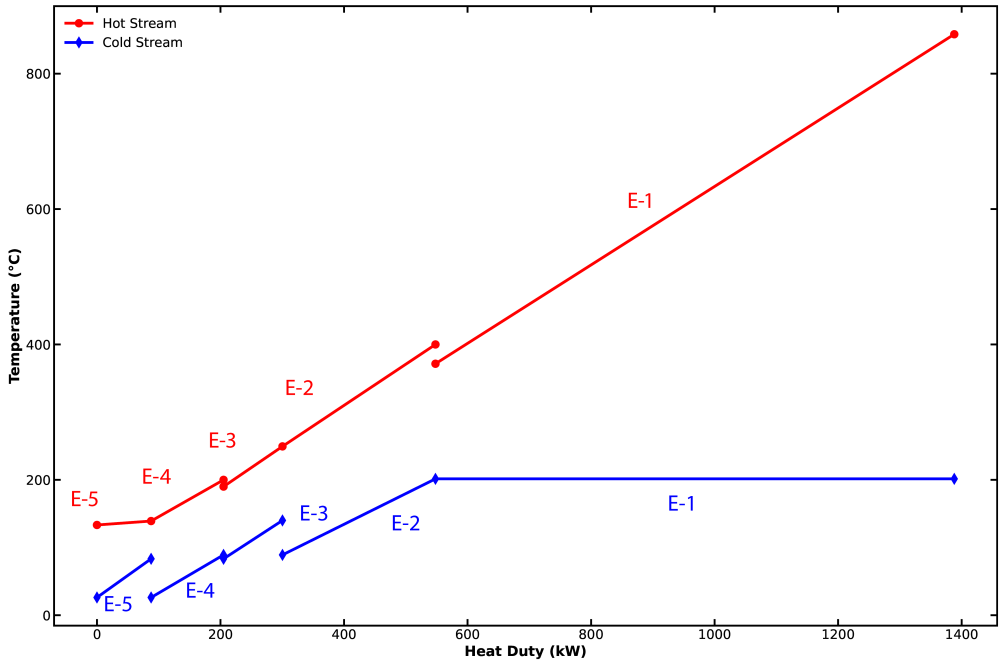

Figure 4.2: Electrified SMR: heat exchanger enthalpies. Heat integration values correspond to the the overall process flowsheet in Fig. 3.7

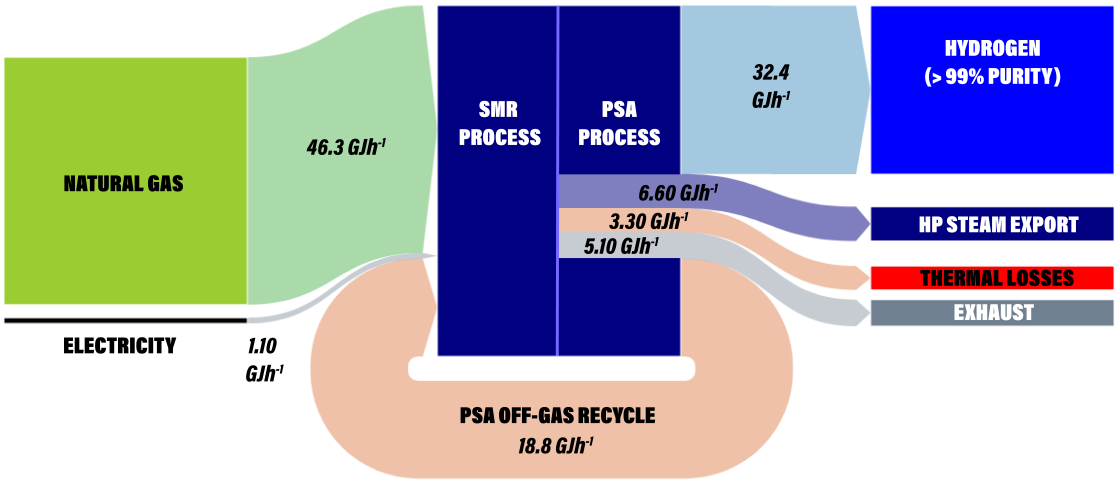

(a) Conventional SMR with natural gas feeds for SMR reactions and combustion heating.

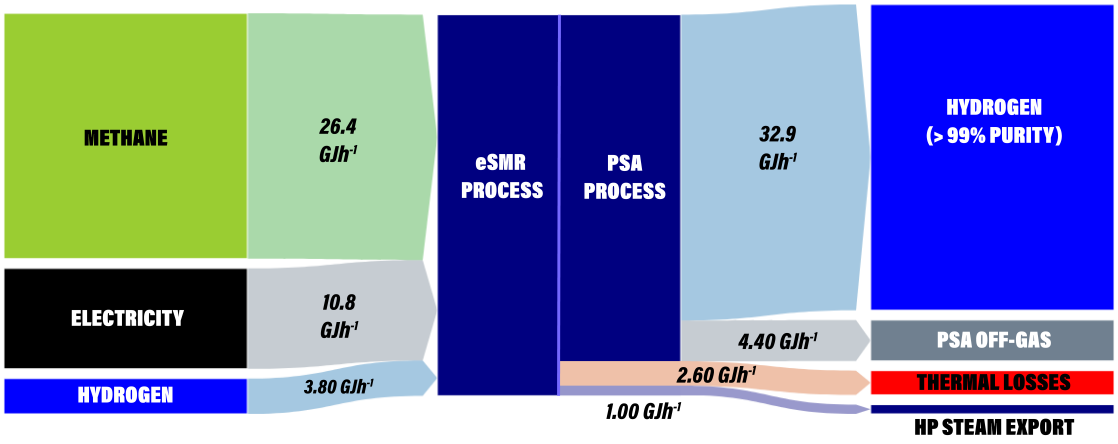

(b) Electrified reforming process with a pure methane feed.

Figure 4.3: Energy utilization diagrams for conventional and electrified processes with 253 kg/h H_2 production rates.

Chapter 5

Conclusion

The SMR process is the cornerstone of industrial H_2 production. Despite its widespread adoption, traditional SMR processes rely on fossil fuels for supplying heat energy, contributing significantly to greenhouse gas emissions. Motivated by a need to change the way heat is supplied to SMR processes, this work focused on an electrically-heated steam methane reformer process, and using experimental results from an electrically-heated steam methane reformer at UCLA, the process was initially modeled with industrial process simulators. Average flux values were configured to match experimental reformer temperatures, space velocities, and pressures to compare the ideal kinetic energy consumption of the reformer to experimental energy data. Based on these data, an Aspen Plus model was constructed and tailored for an industrial-scale hydrogen production process. Finally, a sensitivity analysis was performed to identify energy-efficient operating conditions and compare the conventional SMR process versus the electrified SMR process.

Bibliography

[1] Wolfgang Lubitz and William Tumas. Hydrogen: An overview. *Chemical Reviews*, 107: 3900–3903, 2007.

[2] VA Panchenko, Yu V Daus, AA Kovalev, IV Yudaev, and Yu V Litti. Prospects for the production of green hydrogen: Review of countries with high potential. *International Journal of Hydrogen Energy*, 48:4551–4571, 2023.

[3] Calvin H Bartholomew and Robert J Farrauto. *Fundamentals of industrial catalytic processes*. John Wiley & Sons, 2011.

[4] John C Molburg and Richard D Doctor. Hydrogen from steam-methane reforming with CO_2 capture. In *Proceedings of 20th Annual International Pittsburgh Coal Conference*, 2003.

[5] Peter Häussinger, Reiner Lohmüller, and Allan M. Watson. *Hydrogen, 2. Production*. John Wiley & Sons, Ltd, 2011.

[6] Ankur Kumar, Michael Baldea, and Thomas F Edgar. Real-time optimization of an industrial steam-methane reformer under distributed sensing. *Control Engineering Practice*, 54:140–153, 2016.

[7] DOE. Saving energy with electrical resistance heating, 1997. Department of Energy Report.

[8] Berkay Çıtmacı, Xiaodong Cui, Fahim Abdullah, Derek Richard, Dominic Peters, Yifei Wang, Esther Hsu, Parth Chheda, Carlos G Morales-Guio, and Panagiotis D Christofides.

Model predictive control of an electrically-heated steam methane reformer. *Digital Chemical Engineering*, 10:100138, 2024.

[9] Xiaodong Cui, Berkay Çıtmacı, Dominic Peters, Fahim Abdullah, Yifei Wang, Esther Hsu, Parth Chheda, Carlos G Morales-Guio, and Panagiotis D Christofides. Estimation-based model predictive control of an electrically-heated steam methane reforming process. *Digital Chemical Engineering*, 11:100153, 2024.

[10] Berkay Çıtmacı, Dominic Peters, Xiaodong Cui, Fahim Abdullah, Ahmed Almunaifi, Parth Chheda, Carlos G Morales-Guio, and Panagiotis D Christofides. Feedback control of an experimental electrically-heated steam methane reformer. *Chemical Engineering Research and Design*, 206:469–488, 2024.

[11] Thai Ngan Do, Hweeung Kwon, Minseong Park, Changsu Kim, Yong Tae Kim, and Jiyong Kim. Carbon-neutral hydrogen production from natural gas via electrified steam reforming: Techno-economic-environmental perspective. *Energy Conversion and Management*, 279: 116758, March 2023.

[12] Wei-Hsin Chen and Chia-Yang Chen. Water gas shift reaction for hydrogen production and carbon dioxide capture: A review. *Applied Energy*, 258:114078, 2020.

[13] D Park, GJ Duffy, JH Edwards, DG Roberts, A Ilyushechkin, LD Morpeth, and T Nguyen. Kinetics of high-temperature water-gas shift reaction over two iron-based commercial catalysts using simulated coal-derived syngases. *Chemical Engineering Journal*, 146:148–154, 2009.

[14] Diogo Mendes, Vania Chibante, Adelio Mendes, and Luis M Madeira. Determination of the low-temperature water-gas shift reaction kinetics using a Cu-based catalyst. *Industrial & Engineering Chemistry Research*, 49:11269–11279, 2010.

[15] Howard F. Rase. *Chemical Reactor Design for Process Plants; Volume Two: Case Studies and Design Data*. John Wiley & Sons, 1977.

[16] Alexandre Terrigeol and O Trifilieff. Practical considerations for the design of adsorbent beds–molecular sieve lifetime optimization. In *Gas Processors Association 23rd Annual Technical Conference*, La Garenne Colombes, France, 2015.

[17] Sebastian T Wismann, Jakob S Engbæk, Søren B Vendelbo, Flemming B Bendixen, Winnie L Eriksen, Kim Aasberg-Petersen, Cathrine Frandsen, Ib Chorkendorff, and Peter M Mortensen. Electrified methane reforming: A compact approach to greener industrial hydrogen production. *Science*, 364:756–759, 2019.

[18] U. P. M. Ashik, W. M. A. Wan Daud, and Hazzim F. Abbas. Methane decomposition kinetics and reaction rate over Ni/SiO_2 nanocatalyst produced through co-precipitation cum modified Stöber method. *International Journal of Hydrogen Energy*, 42:938–952, 2017.

[19] Jason M. Ginsburg, Juliana Piña, Tarek El Solh, and Hugo I. de Lasa. Coke formation over a nickel catalyst under methane dry reforming conditions: Thermodynamic and kinetic models. *Industrial & Engineering Chemistry Research*, 44:4846–4854, 2005.

[20] Jianguo Xu and Gilbert F Froment. Methane steam reforming, methanation and water-gas shift: I. Intrinsic kinetics. *AIChE Journal*, 35:88–96, 1989.

[21] Esther Hsu, Dominic Peters, Berkay Çıtmacı, Parth Chheda, Xiaodong Cui, Yifei Wang, Carlos G Morales-Guio, and Panagiotis D Christofides. Modeling and design of a combined electrified steam methane reforming-pressure swing adsorption process. *Chemical Engineering Research and Design*, in press.

[22] Jens Rostrup-Nielsen and Lars J Christiansen. *Concepts in syngas manufacturing*. World Scientific, 2011.

[23] IEA. Comparison of the emissions intensity of different hydrogen production routes, 2021.